First Determination of the Nucleon-Nucleon Response Functions in the Timelike Region

J. G. Messchendorp, J. C. S. Bacelar, M. J. van Goethem, M. N. Harakeh, M. Hoefman, H. Huisman, N. Kalantar-Nayestanaki, H. Löhner, R. W. Ostendorf, S. Schadmand,* O. Scholten, M. Volkerts, and H. W. Wilschut

Kernfysisch Versneller Instituut, Zernikelaan 25, 9747 AA Groningen, The Netherlands

R. S. Simon

Gesellschaft für Schwerionenforschung, Planckstraße 1, D-64291 Darmstadt, Germany

(Received 25 March 1999)

The virtual-bremsstrahlung yields in proton-proton scattering, $pp \to ppe^+e^-$, below the pion threshold were measured. The leptonic-angle dependence of the experimentally determined cross section is exploited in order to extract the nucleon-nucleon response functions in the timelike region. All six response functions are compared to the predictions of a microscopic, fully relativistic nucleon-nucleon model, as well as a model based on a low-energy-theorem expansion.

PACS numbers: 13.75.Cs, 25.10.+s, 25.20.Lj

The knowledge of the strong (NN) interaction between nucleons is the basis of our understanding of nuclear phenomena. For a good description of the NN interaction, experimental and theoretical studies of two interacting nucleons are of importance. Of special interest is bremsstrahlung production in proton-proton collisions, $pp \to pp\gamma$. In this case, charge-exchange contributions are suppressed and increased sensitivity to higher-order diagrams of the NN interaction is obtained. Closely related to the bremsstrahlung process, is the virtual-bremsstrahlung reaction $pp \to ppe^+e^-$. Contrary to real photons, virtual photons possess longitudinal as well as transverse polarization allowing the momentum and energy transfer to be varied independently.

The study of virtual-bremsstrahlung emission during proton-proton collisions provides a complete set of observables to determine details of the NN interaction [1–5]. The virtual-photon polarizations, longitudinal and transverse, as well as their interference terms project the nucleon-nucleon current, which involves the NN T-matrix, onto six independent components, i.e., the nucleon-nucleon response functions. Since the virtual-photon mass is positive, the extracted response functions are in the timelike region. Calculations [3–5] show sensitivity to two-body currents in the magnitude and sign of the transverse responses, whereas the effects of negative-energy states can be observed in the terms containing the longitudinal components. Up to now there has been no determination of these response functions in the timelike region, as opposed to the large volume of data obtained in electron scattering for the spacelike region. The difficulty in the experimental study of this process arises from the fact that the cross section is extremely small. For the experiment discussed here the total measured cross section amounts to 3.2 pb [1]. On the other hand, the response functions are well defined experimentally. The polarization of the virtual photon is determined in a model-independent way solely by the momenta of both leptons. Following Ref. [4], the $pp \to ppe^+e^-$ reaction cross section is expressed as

$$\frac{d^8\sigma}{d\Omega_{p_1} d\Omega_{p_2} dM_\gamma d\theta_\gamma d\cos\theta_\ell d\phi_\ell} = \frac{(m_p e)^4}{(2\pi)^8 j} J|A|^2, \quad (1)$$

where Ω_{p_i} are the solid angles of protons 1 and 2, m_p is the proton mass, j the flux factor, M_γ and θ_γ are the mass and polar angles of the virtual photon, and J is the Jacobian. The angles θ_ℓ and ϕ_ℓ are the polar and azimuthal angles of the momentum-difference vector, ℓ, of the two leptons (k_+, k_-) as shown in Fig. 1. The square of the amplitude, A, is given by [4]

$$|A|^2 = \frac{1}{2M_\gamma^2}\{W_T C_T + W_L C_L + C_{TT}(W_{TT}\cos 2\phi_\ell + W'_{TT}\sin 2\phi_\ell) + C_{LT}(W_{LT}\cos\phi_\ell + W'_{LT}\sin\phi_\ell)\}, \quad (2)$$

where the six independent response functions (W_i), depending only on hadronic variables, and the factors C_i,

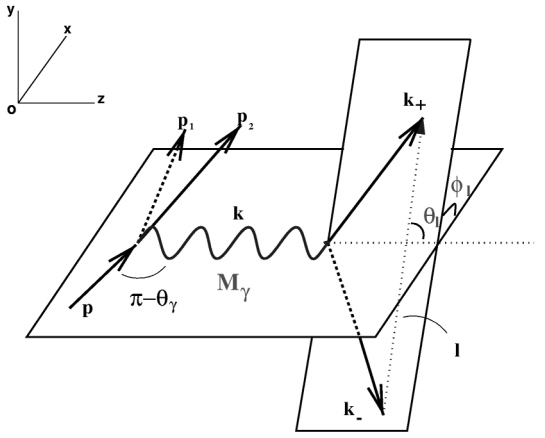

FIG. 1. Schematic view of the virtual-bremsstrahlung emission in proton-proton scattering.

 0031-9007/99/83(13)/2530(4)$15.00

which depend only on leptonic variables, are defined in Table I. Equation (2) demonstrates how to obtain the different response functions separately by measuring the cross section, as functions of M_γ, θ_ℓ, and ϕ_ℓ.

The decomposition of the $pp \to ppe^+e^-$ amplitude into the six response functions is in principle independent of the nucleon-nucleon model used.

The experiment was performed at the Kernfysisch Versneller Instituut using a 190 MeV polarized-proton beam provided by the superconducting cyclotron AGOR. A cylindrically shaped (6 mm thick and 20 mm diameter) liquid-hydrogen target [6], with 4 μm thin Aramid windows, was used. The reaction products were measured in coincidence using the Small-Angle Large-Acceptance Detector (SALAD) [7] and the Two-Arm Photon Spectrometer (TAPS) [8]. SALAD measures the scattering angle of the two outgoing protons in the range $6° < \theta_p < 26°$ as well as their energies. TAPS measured the position and energy of both leptons, resulting in a coverage of the polar angle of the virtual photon between 60° and 180°. The experimental acceptance depends weakly on M_γ. In total 600 $pp \to ppe^+e^-$ events were obtained [1,2], which correspond to a total integrated cross section of $3.2 \pm 0.1(\text{stat}) \pm 0.5(\text{syst})$ pb over the acceptance of the detector. The angular distribution of the virtual photon as well as its invariant-mass dependence have been presented in earlier publications [1,2].

Equation (2) shows that, after integration over the full azimuthal angle ϕ_ℓ, the cross section is determined by the first two terms: the transverse (W_T) and longitudinal (W_L) components. Furthermore, for small angles θ_ℓ, the contribution of W_T will be enhanced relative to W_L. The full data set was divided into two regions of θ_ℓ, each containing the same number of events. To study experimentally the transverse response, W_T, events in the region $\theta_\ell < 40$ (see top panel of Fig. 2) were selected. In Fig. 2, the experimentally determined averaged transverse response function, denoted as $\overline{W}_T$, is shown. The averaging is carried out per invariant-mass bin over the accepted phase space, Ω_{exp} and is defined as

$$\overline{W}_T = \frac{M_\gamma^2}{\xi} \frac{\int_{\Omega_{\text{exp}}} (\frac{d\sigma}{d\Omega})^{\text{exp}}\, d\Omega}{\int_{\Omega_{\text{exp}}} [C_T J]^{\text{th}}\, d\Omega}, \tag{3}$$

where $\xi = (m_p e)^4/(2\pi)^8 j$ [see Eq. (1)]. In practice, the histogram shown in Fig. 2 is obtained by dividing the histogram of all events within the applied θ_ℓ window (the experimental cross section) by one obtained by performing a Monte Carlo integration of $C_T J$ over a model of the experimental acceptance for each bin. The lines in Fig. 2 show the results of a model based on a low-energy theorem (LET) expansion, developed by Korchin *et al.* [4,5]. The amplitude is expressed in terms of a *NN* model describing the pp elastic data. The model takes partially rescattering and meson-exchange currents into account by applying gauge invariance.

To compare the calculation with the data, an event generator simulating the model has been developed. It

TABLE I. Nucleon response functions W_i and the factors C_i determining the $pp \to ppe^+e^-$ cross section. $M_{x,y,z}$ are the covariant nucleonic currents [3–5], for the coordinate system depicted in Fig. 1.

Term	W	C
T	$M_x M_x^* + M_y M_y^*$	$\left(1 - \frac{\ell^2}{2M_\gamma^2} \sin^2\theta_\ell\right)$
L	$\frac{M_\gamma^2}{k_0^2} \lvert M_z\rvert^2$	$\left(1 - \frac{\ell^2}{k_0^2} \cos^2\theta_\ell\right)$
TT	$M_y M_y^* - M_x M_x^*$	
TT'	$-2\text{Re}(M_x M_y^*)$	$\left\{\frac{\ell^2 \sin^2\theta_\ell}{2M_\gamma^2}\right.$
LT	$-2\frac{M_\gamma}{k_0}\text{Re}(M_z M_x^*)$	
LT'	$-2\frac{M_\gamma}{k_0}\text{Re}(M_z M_y^*)$	$\left\{\frac{\ell^2 \sin 2\theta_\ell}{2k_0 M_\gamma}\right.$

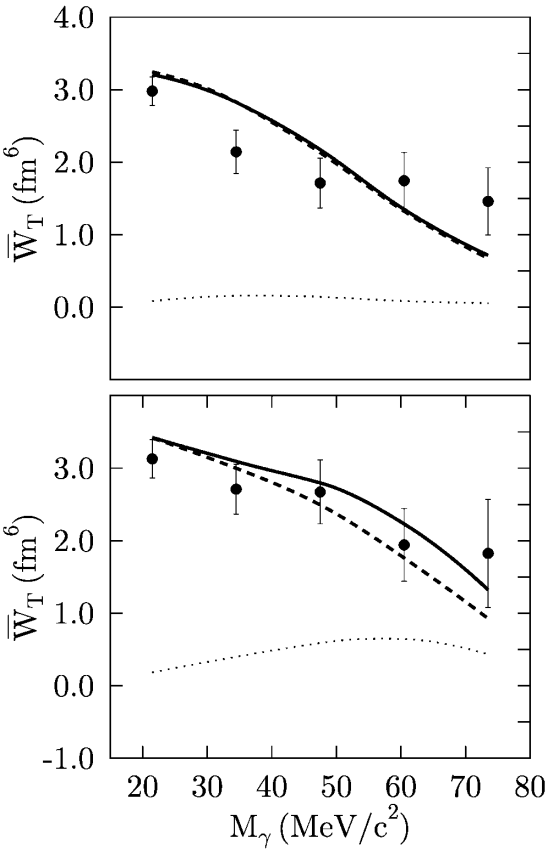

FIG. 2. Experimentally determined average response function $\overline{W}_T$, for events with an energy-sharing angle $\theta_\ell < 40°$ (top panel) and $\theta_\ell > 40°$ (bottom panel). Errors are statistical, and data points are placed at the center of each bin. The results of the LET model [4,5] are shown (solid lines). The contributions from the transverse (dashed lines) and longitudinal (dotted lines) components are shown separately.

is implemented using a four-body decay program [9], generating $pp \rightarrow ppe^+e^-$ events according to phase-space distribution, and by weighting each event with the square of the reaction amplitude, $|A|^2$, obtained from the calculations. The detector response is simulated using GEANT3 [10]. Subsequently, the simulated events are analyzed with the same software constraints as applied to the experimental data. The averaging procedure to obtain the simulated response function, $\overline{W}_T$, is identical to the one used in the analysis of the data. Although not shown in Fig. 2, contributions from the interference terms are not zero, albeit very small, due to the incomplete coverage of the azimuthal angle of the two leptons. Within the statistical (error bars shown in the figure) and systematic accuracy of our data ($\pm 15\%$), the theoretical results for the invariant-mass dependence of $W_T + W_L$ are in agreement with the experimental data. In particular, for the data set with $\theta_\ell > 40°$ (bottom panel of Fig. 2) the strong increase in the W_L component with M_γ is consistent with the data.

Inspecting Eq. (2) it is clear that the measured differential cross section as a function of the azimuthal angle ϕ_ℓ allows the determination of the terms containing the individual interference response functions. To obtain the interference terms (W_{TT}, W_{LT}, W'_{TT}, and W'_{LT}), the amplitudes of the periodic functions $\xi(\phi_\ell)$, chosen from $\cos(2\phi_\ell)$, $\cos(\phi_\ell)$, $\sin(2\phi_\ell)$, or $\sin(\phi_\ell)$, respectively, were extracted from the data. This can be achieved by weighting each event with the value of $\xi(\phi_\ell)$ for that event and integrating over the accepted phase space. As a result, the transverse and longitudinal terms, which do not explicitly depend on ϕ_ℓ, cancel. Also, the contribution from other interference terms cancel due to the orthogonality of the $\xi(\phi_\ell)$ functions. Since the experimental coverage of the azimuthal angle ϕ_ℓ is not complete, this cancellation is not fully achieved. The nonvanishing transverse and longitudinal contributions calculated using the model are subtracted from the data in Fig. 3 which shows the averaged observables, obtained by probing the $\cos(2\phi_\ell)$, $\cos(\phi_\ell)$, $\sin(2\phi_\ell)$, and $\sin(\phi_\ell)$ amplitudes, labeled as $\overline{W}_{TT}$, $\overline{W}_{LT}$, $\overline{W}'_{TT}$, and $\overline{W}'_{LT}$, respectively.

Demonstrating the procedure for $\overline{W}_{TT}$, one defines

$$\overline{W}_{TT} = \frac{M_\gamma^2}{\xi} \frac{\int_{\Omega_{\rm exp}} (\frac{d\sigma}{d\Omega})^{\rm exp} \cos 2\phi_\ell \, d\Omega}{\int_{\Omega_{\rm exp}} \cos^2 2\phi_\ell [C_{TT} J]^{\rm th} \, d\Omega} . \qquad (4)$$

For this observable, the nonvanishing contribution from W_T is calculated with the following integral:

$$\frac{M_\gamma^2}{\xi} \frac{\int_{\Omega_{\rm exp}} \cos 2\phi_\ell [W_T C_{TT} J]^{\rm th} \, d\Omega}{\int_{\Omega_{\rm exp}} \cos^2 2\phi_\ell [C_{TT} J]^{\rm th} \, d\Omega} . \qquad (5)$$

To extract the interference terms W'_{TT} and W'_{LT}, one has to realize that parity conservation, i.e., a reflection in the xz plane (see Fig. 1), requires that $W'_{TT} \rightarrow -W'_{TT}$ and $W'_{LT} \rightarrow -W'_{LT}$ [see Eq. (2)]. Since the response functions depend only on the nucleonic degrees of freedom, the latter implies that W'_{TT} and W'_{LT} change sign with the noncoplanarity angle of the event [3–5], to compensate the change of sign of $\sin\phi_\ell$ and $\sin 2\phi_\ell$. Therefore, the change of sign is applied for these terms as an additional weight function. Without this action, these two terms would integrate out to zero over the full phase space. Exactly the same procedure is applied to the microscopic calculations using the Monte Carlo technique.

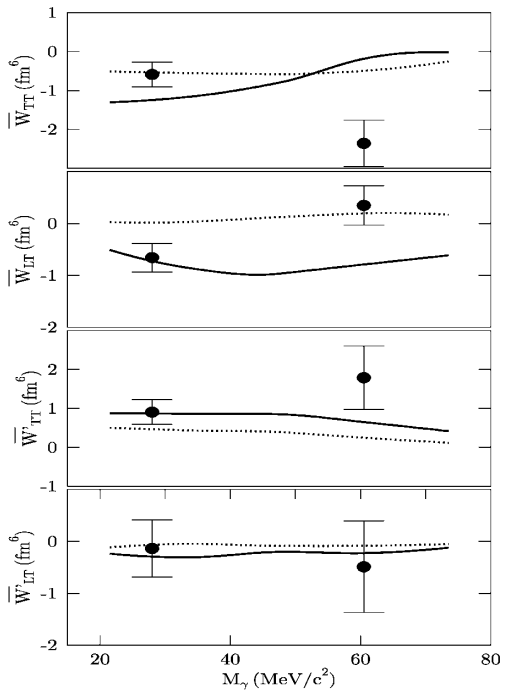

FIG. 3. The interference terms $\overline{W}_{TT}$, $\overline{W}_{LT}$, $\overline{W}'_{TT}$, and $\overline{W}'_{LT}$. The data are shown for two M_γ bins: $15 < M_\gamma < 40$ and $40 < M_\gamma < 80$ MeV/c^2, and the points placed at the center of each bin. The solid lines are the predictions of a microscopic calculation [3], and the dashed lines the predictions of the LET model [4,5].

The solid lines in Fig. 3 are the result of a fully relativistic microscopic calculation by Martinus [3] based on the Fleischer-Tjon potential [11]. This model includes the off-shell dynamics of the interacting protons. Furthermore, it takes explicitly into account the rescattering contributions, the meson-exchange currents, and the virtual Δ isobar. The dashed lines are the predictions of the LET model. It is observed that for small photon masses ($15 < M_\gamma < 40$ MeV/c^2), the measured response functions are in general in good agreement with the predictions of both calculations, both in sign and magnitude. An exception is the overestimation by the microscopic model of the W_{TT} response, which is connected with a similar discrepancy, also by a factor of 2, found for W_T (i.e., the differential cross sections discussed in Refs. [1,2]), as well as for the real photon amplitude [7]. However the larger magnitude predicted for the longitudinal terms (in particular, W_{LT}) seems to be in better agreement with our data. Significant deviations are found at large invariant masses ($40 < M_\gamma < 80$ MeV/c^2), for

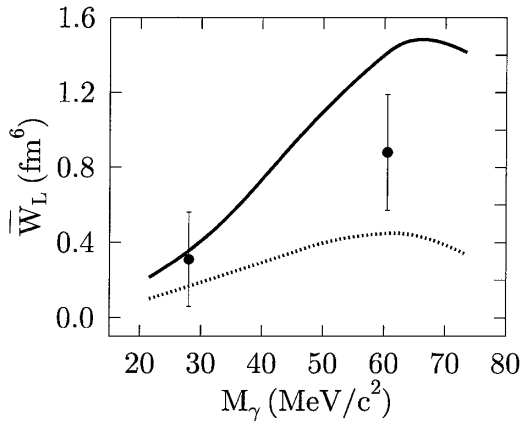

FIG. 4. The determination of $\overline{W}_L$. The binning of the data and the curves are explained in the caption of Fig. 3.

W_{TT}, W_{LT}, and W'_{TT}, for both models. It is noted that for this high invariant-mass region, $\overline{W}_{TT}$ ($\overline{W}_{LT}$) contains significant contributions from the term W_{LT} (W_{TT}). This is caused by the limited acceptance of the azimuthal angle ϕ_ℓ at large electron-positron opening angles, and therefore, large photon masses.

To complete the determination of all six response functions, Fig. 4 shows the results for $\overline{W}_L$. These are obtained from the data set with $\theta_\ell > 40$. The nonvanishing contributions of W_T, W_{TT}, and W_{LT} were subtracted from the data points shown in the bottom panel of Fig. 2. The data are compared in Fig. 4 with the predictions of both models. As pointed out above, the data clearly show the expected increase of W_L with increasing M_γ, although it is not sufficiently accurate to differentiate between the two model predictions. This is the first determination of the longitudinal nucleonic currents.

In summary, the response functions of the $pp \to ppe^+e^-$ amplitude in the timelike region are extracted for the first time from an analysis of the azimuthal dependence of the virtual-bremsstrahlung yields. The extracted values are compared with a fully relativistic microscopic calculation, as well as an LET calculation. It is shown that at low invariant masses the interference response functions are well predicted by the models both in sign and magnitude. In particular, the special new feature associated with virtual bremsstrahlung, the longitudinal responses, are well reproduced by the microscopic model over the entire invariant-mass range. However, there are statistically significant discrepancies between theory and data for the interference response functions, which clearly require improvements in the theoretical description of the nucleonic currents.

The authors acknowledge the support by the TAPS collaboration, and thank A. Yu. Korchin and R. Timmermans for useful discussions. This work is part of the research program of the "Stichting voor Fundamenteel Onderzoek der Materie" (FOM) with financial support from the "Nederlandse Organisatie voor Wetenschappelijk Onderzoek" (NWO), and by the European Union HCM network under Contract No. HRXCT94066.

*Present address: Universität Giessen, Heinrich-Buff-Ring 16, 35392 Giessen, Germany.

[1] J. G. Messchendorp *et al.*, Phys. Rev. Lett. **82**, 2649 (1999).
[2] J. G. Messchendorp *et al.*, Nucl. Phys. **A631**, 618c (1998).
[3] G. H. Martinus, Ph.D. thesis, University of Groningen, 1998; *"Few Body Systems 1999"* (to be published).
[4] A. Yu. Korchin and O. Scholten, Nucl. Phys. **A581**, 493 (1995).
[5] A. Yu. Korchin, O. Scholten, and D. Van Neck, Nucl. Phys. **A602**, 423 (1996).
[6] N. Kalantar-Nayestanaki *et al.*, Nucl. Instrum. Methods Phys. Res., Sect. A **417**, 215 (1998).
[7] N. Kalantar-Nayestanaki, Nucl. Phys. **A631**, 242c (1998).
[8] A. R. Gabler *et al.*, Nucl. Instrum. Methods Phys. Res., Sect. A **346**, 168 (1994).
[9] F. James, CERN Report No. 68-15, 1968.
[10] R. Brun, F. Bruyant, A. C. McPherson, and P. Zanarini, GEANT3 Users Guide, Data Handling Division DD/EE/84-1, CERN, 1986.
[11] J. Fleischer and J. Tjon, Nucl. Phys. **B84**, 375 (1975).